



Measurement of the effective $B_s^0 \rightarrow K^+ K^-$ lifetime [☆]

LHCb Collaboration

ARTICLE INFO

Article history:

Received 2 November 2011
Received in revised form 20 December 2011
Accepted 22 December 2011
Available online 28 December 2011
Editor: W.-D. Schlatter

ABSTRACT

A measurement of the effective $B_s^0 \rightarrow K^+ K^-$ lifetime is presented using approximately 37 pb^{-1} of data collected by LHCb during 2010. This quantity can be used to put constraints on contributions from processes beyond the Standard Model in the B_s^0 meson system and is determined by two complementary approaches as

$$\tau_{KK} = 1.440 \pm 0.096 \text{ (stat)} \pm 0.008 \text{ (syst)} \pm 0.003 \text{ (model)} \text{ ps.}$$

© 2011 CERN. Published by Elsevier B.V. Open access under CC BY-NC-ND license.

1. Introduction

The study of charmless B meson decays of the form $B \rightarrow h^+ h'^-$, where $h^{(\prime)}$ is either a kaon, pion or proton, offers a rich opportunity to explore the phase structure of the CKM matrix and to search for manifestations of physics beyond the Standard Model. The effective lifetime, defined as the decay-time expectation value, of the B_s^0 meson measured in the decay channel $B_s^0 \rightarrow K^+ K^-$ (charge conjugate modes are implied throughout the Letter) is of considerable interest as it can be used to put constraints on contributions from new physical phenomena to the B_s^0 meson system [1–4]. The $B_s^0 \rightarrow K^+ K^-$ decay was first observed by CDF [5,6]. The decay has subsequently been confirmed by Belle [7].

The detailed formalism of the effective lifetime in $B_s^0 \rightarrow K^+ K^-$ decay can be found in Refs. [3,4]. The untagged decay-time distribution can be written as

$$\Gamma(t) \propto (1 - \mathcal{A}_{\Delta\Gamma_s})e^{-\Gamma_L t} + (1 + \mathcal{A}_{\Delta\Gamma_s})e^{-\Gamma_H t}. \quad (1)$$

The parameter $\mathcal{A}_{\Delta\Gamma_s}$ is defined as $\mathcal{A}_{\Delta\Gamma_s} = -2 \text{Re}(\lambda)/(1 + |\lambda|^2)$ where $\lambda = (q/p)(\bar{A}/A)$ and the complex coefficients p and q define the mass eigenstates of the $B_s^0 - \bar{B}_s^0$ system in terms of the flavour eigenstates (see, e.g., Ref. [8]), while A (\bar{A}) gives the amplitude for B_s^0 (\bar{B}_s^0) decay to the CP even $K^+ K^-$ final state. In the absence of CP violation, $\text{Re}(\lambda) = 1$ and $\text{Im}(\lambda) = 0$, so that the distribution involves only the term containing Γ_L . Any deviation from a pure single exponential with decay constant Γ_L^{-1} is a measure of CP violation.

When modelling the decay-time distribution shown in Eq. (1) with a single exponential function in a maximum likelihood fit, it converges to the effective lifetime given in Eq. (2) [9]. For

small values of the relative width difference $\Delta\Gamma_s/\Gamma_s = (\Gamma_L - \Gamma_H)/((\Gamma_L + \Gamma_H)/2)$, the distribution can be approximated by Taylor expansion as shown in the second part of the equation [3]

$$\begin{aligned} \tau_{KK} &= \tau_{B_s^0} \frac{1}{1 - y_s^2} \left[\frac{1 + 2\mathcal{A}_{\Delta\Gamma_s} y_s + y_s^2}{1 + \mathcal{A}_{\Delta\Gamma_s} y_s} \right] \\ &= \tau_{B_s^0} (1 + \mathcal{A}_{\Delta\Gamma_s} y_s + \mathcal{O}(y_s^2)), \end{aligned} \quad (2)$$

where $\tau_{B_s^0} = 2/(\Gamma_H + \Gamma_L) = \Gamma_s^{-1}$ and $y_s = \Delta\Gamma_s/2\Gamma_s$. The Standard Model predictions for these parameters are $\mathcal{A}_{\Delta\Gamma_s} = 0.97_{-0.009}^{+0.014}$ [3] and $y_s = 0.066 \pm 0.016$ [10].

The decay $B_s^0 \rightarrow K^+ K^-$ is dominated by loop diagrams carrying, in the Standard Model, the same phase as the $B_s^0 - \bar{B}_s^0$ mixing amplitude and hence the measured effective lifetime is expected to be close to Γ_L^{-1} . The tree contribution to the $B_s^0 \rightarrow K^+ K^-$ decay amplitude, however, introduces CP violation effects. The Standard Model prediction is $\tau_{KK} = 1.390 \pm 0.032 \text{ ps}$ [3]. In the presence of physics beyond the Standard Model, deviations of the measured value from this prediction are possible.

The measurement has been performed using a data sample corresponding to an integrated luminosity of 37 pb^{-1} collected by LHCb at an energy of $\sqrt{s} = 7 \text{ TeV}$ during 2010. A key aspect of the analysis is the correction of lifetime biasing effects, referred to as the acceptance, which are introduced by the selection criteria to enrich the B meson sample. Two complementary data-driven approaches have been developed to compensate for this bias. One method relies on extracting the acceptance function from data, and then applies this acceptance correction to obtain a measurement of the $B_s^0 \rightarrow K^+ K^-$ lifetime. The other approach cancels the acceptance bias by taking the ratio of the $B_s^0 \rightarrow K^+ K^-$ lifetime distribution with that of $B^0 \rightarrow K^+ \pi^-$.

[☆] © CERN for the benefit of the LHCb Collaboration.

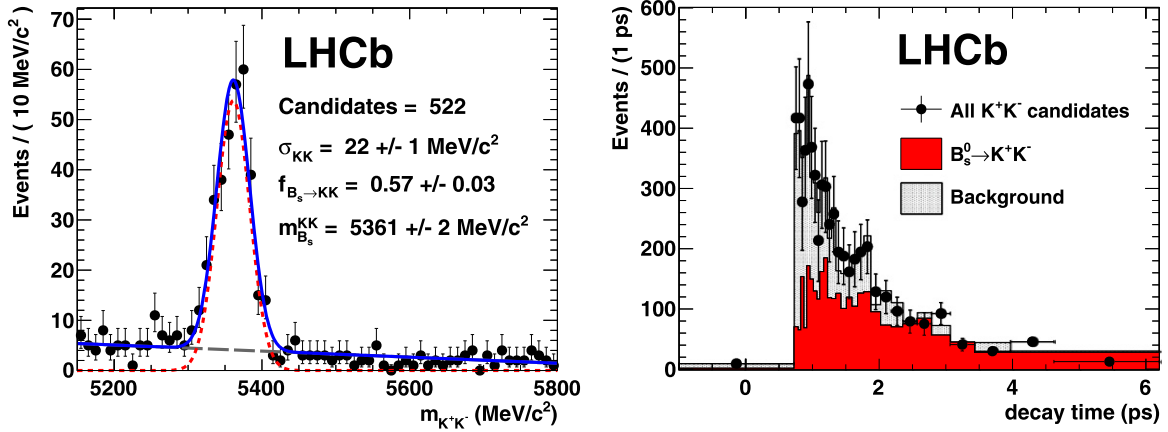


Fig. 1. Results of the relative lifetime fit. Left: Fit to the time-integrated KK mass spectrum. Right: Fit to the KK decay-time distribution. The black points show the total number of candidates per picosecond in each decay time bin, the stacked histogram shows the $B_s^0 \rightarrow K^+K^-$ yield in red (dark) and the background yield in grey (light). (For interpretation of the references to colour in this figure legend, the reader is referred to the web version of this Letter.)

2. Data sample

The LHCb detector [11] is a single arm spectrometer with a pseudorapidity acceptance of $2 < \eta < 5$ for charged particles. The detector includes a high precision tracking system which consists of a silicon vertex detector and several dedicated tracking planes with silicon microstrip detectors (Inner Tracker) covering the region with high charged particle multiplicity and straw tube detectors (Outer Tracker) for the region with lower occupancy. The Inner and Outer trackers are placed after the dipole magnet to allow the measurement of the charged particles' momenta as they traverse the detector. Excellent particle identification capabilities are provided by two ring imaging Cherenkov detectors which allow charged pions, kaons and protons to be distinguished from each other in the momentum range 2–100 GeV/c. The experiment employs a multi-level trigger to reduce the readout rate and enhance signal purity: a hardware trigger based on the measurement of the energy deposited in the calorimeter cells and the momentum transverse to the beamline of muon candidates, as well as a software trigger which allows the reconstruction of the full event information.

B mesons are produced with an average momentum of around 100 GeV/c and have decay vertices displaced from the primary interaction vertex. Background particles tend to have low momentum and tend to originate from the primary pp collision. These features are exploited in the event selection. In the absolute lifetime measurement the final event selection is designed to be more stringent than the trigger requirements, as this simplifies the calculation of the candidate's acceptance function. The tracks associated with the final state particles of the B meson decay are required to have a good track fit quality ($\chi^2/\text{ndf} < 3$ for one of the two tracks and $\chi^2/\text{ndf} < 4$ for the other), have high momentum ($p > 13.5$ GeV/c), and at least one particle must have a transverse momentum of more than 2.5 GeV/c. The primary proton–proton interaction vertex (or vertices in case of multiple interactions) of the event is fitted from the reconstructed charged particles. The reconstructed trajectory of at least one of the final state particles is required to have a distance of closest approach to all primary vertices of at least 0.25 mm.

The B meson candidate is obtained by reconstructing the vertex formed by the two-particle final state. The B meson transverse momentum is required to be greater than 0.9 GeV/c and the distance of the decay vertex to the closest primary pp interaction vertex has to be larger than 2.4 mm. In the final stage of the selection the modes $B_s^0 \rightarrow K^+K^-$ and $B^0 \rightarrow K^+\pi^-$ are separated

by pion/kaon likelihood variables which use information obtained from the ring imaging Cherenkov detectors.

The event selection used in the relative lifetime analysis is very similar. However, some selection criteria can be slightly relaxed as the analysis does not depend on the exact trigger requirements.

3. Relative lifetime measurement

This analysis exploits the fact that the kinematic properties of the $B_s^0 \rightarrow K^+K^-$ decay are very similar to those of $B^0 \rightarrow K^+\pi^-$. The two different decay modes can be separated using information from the ring imaging Cherenkov detectors. The left part of Fig. 1 shows the invariant mass distribution of the $B_s^0 \rightarrow K^+K^-$ candidates after the final event selection. In addition 1,424 $B^0 \rightarrow K^+\pi^-$ candidates are selected. Using a data-driven particle identification calibration method described in the systematics section, the remaining contamination in the $B_s^0 \rightarrow K^+K^-$ sample from other $B \rightarrow h^+h'^-$ final states in the analysed mass region is estimated to be 3.8%.

B mesons in either channel can be selected using identical kinematic constraints and hence their decay-time acceptance functions are almost identical. Therefore the effects of the decay-time acceptance cancel in the ratio and the effective $B_s^0 \rightarrow K^+K^-$ lifetime can be extracted relative to the $B^0 \rightarrow K^+\pi^-$ mode from the variation of the ratio $R(t)$ of the yield of B meson candidates in both decay modes with decay time:

$$R(t) = R(0)e^{-t(\tau_{KK}^{-1} - \tau_{K\pi}^{-1})}. \quad (3)$$

The cancellation of acceptance effects has been verified using simulated events, including the full simulation of detector effects, trigger response and final event selection. Any non-cancelling acceptance bias on the measured lifetime is found to be smaller 1 fs.

In order to extract the effective $B_s^0 \rightarrow K^+K^-$ lifetime, the yield of B meson candidates is determined in bins of decay time for both decay modes. Thirty bins between -1 ps and 35 ps are chosen such that each bin contains approximately the same number of B meson candidates. The ratio of the yields is then fitted as a function of decay time and the relative lifetime can be determined according to Eq. (3). With this approach it is not necessary to parametrise the decay-time distribution of the background. In order to maximise the statistical precision, both steps of the analysis are combined in a simultaneous fit to the K^+K^- and $K^+\pi^-$ invariant mass spectra across all decay-time bins. The signal distributions are described by Gaussian functions and the combinatorial

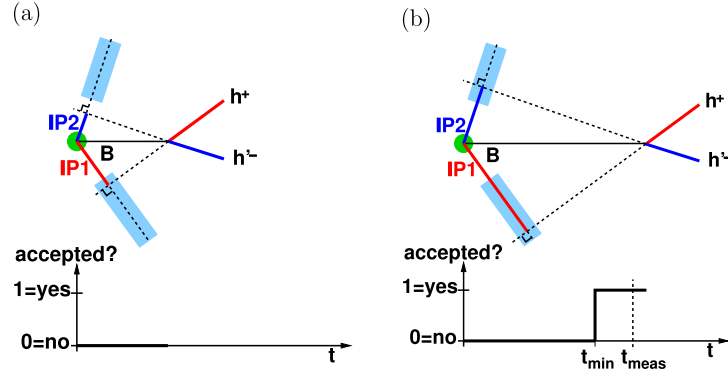


Fig. 2. Decay-time acceptance function for an event of a two-body hadronic decay. The light blue (shaded) regions show the bands for accepting the impact parameter of a track. The impact parameter of the negative track (IP2) is too small in (a) and lies within the accepted range in (b). The actual measured decay time lies in the accepted region. The acceptance intervals give conditional likelihoods used in the lifetime fit. (For interpretation of the references to colour in this figure legend, the reader is referred to the web version of this Letter.)

background by first order polynomials. The parameters of the signal and background probability density functions (PDFs) are fixed to the results of time-integrated mass fits before the lifetime fit is performed. The $B^0 \rightarrow K^+\pi^-$ yield ($N_{B \rightarrow K\pi}$) is allowed to float freely in each bin but the $B_s^0 \rightarrow K^+K^-$ yield ($N_{B_s \rightarrow KK}$) is constrained to follow

$$N_{B_s \rightarrow KK}(\bar{t}_i) = N_{B \rightarrow K\pi}(\bar{t}_i) R(0) e^{-\bar{t}_i(\tau_{KK}^{-1} - \tau_{K\pi}^{-1})}, \quad (4)$$

where \bar{t}_i is the mean decay time in the i th bin. In total the simultaneous fit has 94 free parameters and tests using Toy Monte Carlo simulated data have found the fit to be unbiased to below 1 fs on the measured $B_s^0 \rightarrow K^+K^-$ lifetime. Each mass fit used in the simultaneous fit is unbinned and must be splitted into mass bins in order to evaluate the fit χ^2 . Two mass bins are chosen, one signal dominated and one background dominated, in order to guarantee a minimum of 5–6 candidates in each bin. Using this approach the χ^2 per degree of freedom of the simultaneous fit is found to be 0.82. The right part of Fig. 1 shows the decay-time distribution obtained from the fit and the fitted reciprocal lifetime difference is

$$\tau_{KK}^{-1} - \tau_{K\pi}^{-1} = 0.013 \pm 0.045 \text{ (stat) ps}^{-1}.$$

Taking the $B^0 \rightarrow K^+\pi^-$ lifetime as equal to the mean B^0 lifetime ($\tau_{B^0} = 1.519 \pm 0.007$ ps) [8], this measurement can be expressed as

$$\tau_{KK} = 1.490 \pm 0.100 \text{ (stat)} \pm 0.007 \text{ (input) ps}$$

where the second uncertainty originates from the uncertainty of the B^0 lifetime.

4. Absolute lifetime measurement

The absolute lifetime measurement method directly determines the effective $B_s^0 \rightarrow K^+K^-$ lifetime using an acceptance correction calculated from the data. This method was first used at the NA11 spectrometer at CERN SPS [12], further developed within CDF [13,14] and was subsequently studied and implemented in LHCb [15,16]. The *per-event* acceptance function is determined by evaluating whether the candidate would be selected for different values of the B meson candidate decay time. For example, for a B meson candidate, with given kinematic properties, the measured decay time of the B meson candidate is directly related to the point of closest approach of the final state particles to the associated primary vertex. Thus a selection requirement on this quantity directly translates into a discrete decision about acceptance or rejection of a candidate as a function of its decay time.

This is illustrated in Fig. 2. In the presence of several reconstructed primary interaction vertices, the meson may enter a decay-time region where one of the final state particles no longer fulfils the selection criteria with respect to another primary vertex. Hence the acceptance function is determined as a series of step changes. These *turning points* at which the candidates enter or leave the acceptance of a given primary vertex form the basis of extracting the *per-event* acceptance function in the data. The turning points are determined by moving the reconstructed primary vertex position of the event along the B meson momentum vector, and then reapplying the event selection criteria. The analysis presented in this Letter only includes events with a single turning point. The drop of the acceptance to zero when the final state particles are so far downstream that one is outside the detector acceptance occurs only after many lifetimes and hence is safely neglected.

The distributions of the turning points, combined with the decay-time distributions, are converted into an average acceptance function (see Fig. 3). The average acceptance is not used in the lifetime fit, except in the determination of the background decay-time distribution.

The effective $B_s^0 \rightarrow K^+K^-$ lifetime is extracted by an unbinned maximum likelihood fit using an analytical probability density function (PDF) for the signal decay time and a non-parametric PDF for the combinatorial background, as described below. The measurement is factorised into two independent fits.

A first fit is performed to the observed mass spectrum and used to determine the signal and background probabilities of each event. Events with B_s^0 candidates in the mass range 5272–5800 MeV/ c^2 were used, hence reducing the contribution of partially reconstructed background and contamination of B^0 decays below the B_s^0 mass peak. The signal distribution is modelled with a Gaussian, and the background with a linear distribution. The fitted mass value is compatible with the current world average [8].

The signal and background probabilities are used in the subsequent lifetime fit. The decay-time PDF of the signal is calculated analytically taking into account the *per-event* acceptance and the decay-time resolution. The decay-time PDF of the combinatorial background is estimated from data using a non-parametric method and is modelled by a sum of kernel functions which represent each candidate by a normalised Gaussian function centred at the measured decay time with a width proportional to an estimate of the density of candidates at this decay time [17]. The lifetime fit is performed in the decay-time range of 0.6–15 ps, hence only candidates within this range were accepted. The analysis was tested on the $B^0 \rightarrow K^+\pi^-$ channel, for which a lifetime compatible with the world average value was obtained, and applied to the $B_s^0 \rightarrow K^+K^-$

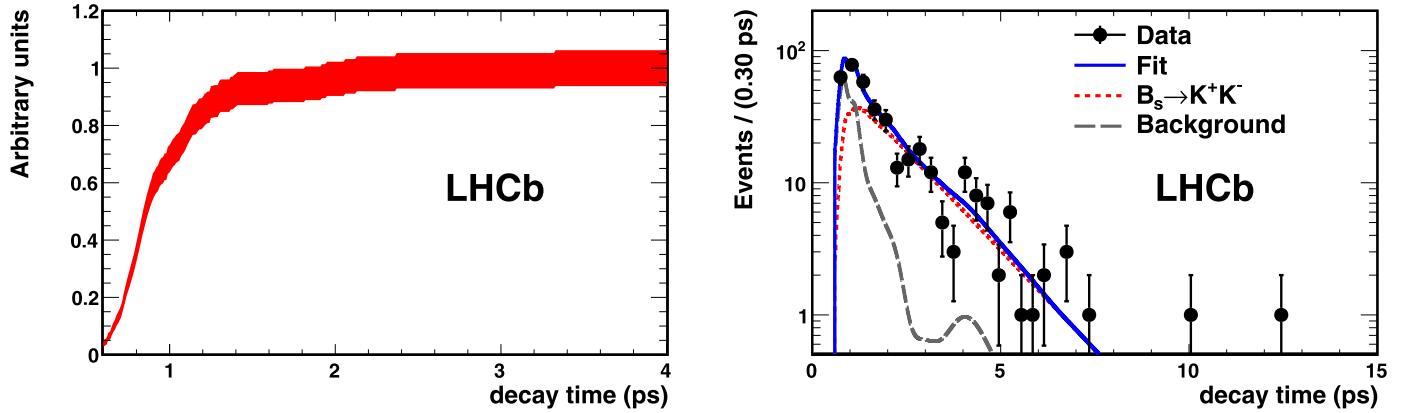


Fig. 3. Left: Average decay-time acceptance function for signal events, where the error band is an estimate of the statistical uncertainty. The plot is scaled to 1 at large decay times, not taking into account the total signal efficiency. Right: Decay-time distribution of the $B_s^0 \rightarrow K^+ K^-$ candidates and the fitted functions. The estimation of the background distribution is sensitive to fluctuations due to the limited statistics. Both plots are for the absolute lifetime measurement. (For interpretation of the references to colour in this figure legend, the reader is referred to the web version of this Letter.)

Table 1
Summary of systematic uncertainties on the $B_s^0 \rightarrow K^+ K^-$ lifetime measurements.

Source of uncertainty	Uncertainty on τ_{KK} (fs)	Uncertainty on $\tau_{KK}^{-1} - \tau_{K\pi}^{-1}$ (ns ⁻¹)
Fit method	3.2	0.5
Acceptance correction	6.3	
Mass model	1.9	
$B \rightarrow h^+ h'^-$ background	1.9	1.4
Partially reconstructed background	1.9	1.1
Combinatorial background	1.5	1.6
Primary vertex association	1.2	0.5
Detector length scale	1.5	0.7
Production asymmetry	1.4	0.6
Minimum accepted lifetime	1.1	N/A
Total (added in quadrature)	8.4	2.7
Effective lifetime interpretation	2.8	1.1

channel only once the full analysis procedure had been fixed. The result of the lifetime fit is

$$\tau_{KK} = 1.440 \pm 0.096 \text{ (stat) ps}$$

and is illustrated in Fig. 3.

5. Systematic uncertainties

The systematic uncertainties are listed in Table 1 and discussed below. The dominant contributions to the systematic uncertainty for the absolute lifetime measurement come from the treatment of the acceptance correction (6.3 fs) and the fitting procedure (3.2 fs). The systematic uncertainty from the acceptance correction is determined by applying the same analysis technique to a kinematically similar high statistics decay in the charm sector ($D^0 \rightarrow K^- \pi^+$ [18]). This analysis yields a lifetime value in good agreement with the current world average and of better statistical accuracy. The uncertainty on the comparison between the measured value and the world average is rescaled by the B meson and charm meson lifetime ratio. The uncertainty due to the fitting procedure is evaluated using simplified simulations. A large number of pseudo-experiments are simulated and the pull of the fitted lifetimes compared to the input value to the fit is used to estimate the accuracy of the fit. These sources of uncertainty are not dominant in the relative method, and are estimated from simplified simulations which also include the systematic uncertainty of the mass model. Hence a common systematic uncertainty is assigned to these three sources.

The effect of the contamination of other $B \rightarrow h^+ h'^-$ modes to the signal modes is determined by a data-driven method. The

misidentification probability of protons, pions and kaons is measured in data using the decays $K_S^0 \rightarrow \pi^+ \pi^-$, $D^0 \rightarrow K^+ \pi^-$, $\phi \rightarrow K^+ K^-$ and $\Lambda \rightarrow p \pi^-$, where the particle type is inferred from kinematic constraints alone [19]. As the particle identification likelihood separating protons, kaons and pions depends on kinematic properties such as momentum, transverse momentum, and number of reconstructed primary interaction vertices, the sample is reweighted to reflect the different kinematic range of the final state particles in $B \rightarrow h^+ h'^-$ decays. The effect on the measured lifetime is evaluated with simplified simulations.

Decays of B_s^0 and B^0 to three or more final state particles, which have been partially reconstructed, lie predominantly in the mass range below the B_s^0 mass peak outside the analysed region. Residual background from this source is estimated from data and evaluated with a sample of fully simulated partially reconstructed decays. The effect on the fitted lifetime is then evaluated.

In the absolute lifetime measurement, the combinatorial background of the decay-time distribution is described by a non-parametric function, based on the observed events with masses above the B_s^0 meson signal region. The systematic uncertainty is evaluated by varying the region used for evaluating the combinatorial background. In the relative lifetime measurement, the combinatorial background in the hh' invariant mass spectrum is described by a first order polynomial. To estimate the systematic uncertainty, a sample of simulated events is obtained with a simplified simulation using an exponential function, and subsequently fitted with a first order polynomial.

Events may contain several primary interactions and a reconstructed B meson candidate may be associated to the wrong primary vertex. This effect is studied using the more abundant charm meson decays where the lifetime is measured separately for events with only one or any number of primary vertices and the observed variation is scaled to the B meson system.

Particle decay times are measured from the distance between the primary vertex and secondary decay vertex in the silicon vertex detector. The systematic uncertainty from this source is determined by considering the potential error on the length scale of the detector from the mechanical survey, thermal expansion and the current alignment precision.

The analysis assumes that B_s^0 and \bar{B}_s^0 mesons are produced in equal quantities. The influence of a production asymmetry for B_s^0 mesons on the measured lifetime is found to be small.

In the absolute lifetime method both a Gaussian and a Crystal Ball mass model [20] are implemented and the effect on fully simulated data is evaluated to estimate the systematic uncertainty due to the modelling of the signal PDF. In the relative lifetime method

this uncertainty is evaluated with simplified simulations and included in the fitting procedure uncertainty.

In the absolute $B_s^0 \rightarrow K^+K^-$ lifetime measurement a cut is applied on the minimal reconstructed decay time. As the background decay-time estimation will smear this step in the distribution, a systematic uncertainty is quoted from varying this cut.

There is an additional uncertainty introduced if the result is interpreted using Eq. (2), as this expression does not take into account detector resolution and decay-time acceptance. This effect was studied using simplified simulations modelling the acceptance observed in the data and conservative values of $\Delta\Gamma_s = 0.1$ ps and $\mathcal{A}_{\Delta\Gamma_s} = -0.6$. The observed bias with respect to the prediction of Eq. (2) is 3 fs. This effect is labelled “Effective lifetime interpretation” in Table 1 and is not a source of systematic uncertainty on the measurement but is relevant to the interpretation of the measured lifetime.

6. Results and conclusions

The effective $B_s^0 \rightarrow K^+K^-$ lifetime has been measured in pp interactions using a data sample corresponding to an integrated luminosity of 37 pb^{-1} recorded by the LHCb experiment in 2010. Two complementary approaches have been followed to compensate for acceptance effects introduced by the trigger and final event selection used to enrich the sample of B_s^0 mesons. The absolute measurement extracts the *per-event* acceptance function directly from the data and finds:

$$\tau_{KK} = 1.440 \pm 0.096 \text{ (stat)} \pm 0.008 \text{ (syst)} \pm 0.003 \text{ (model)} \text{ ps}$$

where the third source of uncertainty labelled “model” is related to the interpretation of the effective lifetime.

The relative method exploits the fact that the kinematic properties of the various $B \rightarrow h^+h'^-$ modes are almost identical and extracts the $B_s^0 \rightarrow K^+K^-$ lifetime relative to the $B^0 \rightarrow K^+\pi^-$ lifetime as:

$$\tau_{KK}^{-1} - \tau_{K\pi}^{-1} = 0.013 \pm 0.045 \text{ (stat)} \pm 0.003 \text{ (syst)} \\ \pm 0.001 \text{ (model)} \text{ ps}^{-1}.$$

Taking the $B^0 \rightarrow K^+\pi^-$ lifetime as equal to the mean B^0 lifetime ($\tau_{B^0} = 1.519 \pm 0.007$ ps) [8], this measurement can be expressed as:

$$\tau_{KK} = 1.490 \pm 0.100 \text{ (stat)} \pm 0.006 \text{ (syst)} \pm 0.002 \text{ (model)} \\ \pm 0.007 \text{ (input)} \text{ ps},$$

where the last uncertainty originates from the uncertainty of the B^0 lifetime. Both measurements are found to be compatible with each other, taking the overlap in the data analysed into account.

Due to the large overlap of the data analysed by the two methods and the high correlation of the systematic uncertainties, there is no significant gain from a combination of the two numbers. Instead, the result obtained using the absolute lifetime method is taken as the final result. The measured effective $B_s^0 \rightarrow K^+K^-$

lifetime is in agreement with the Standard Model prediction of $\tau_{KK} = 1.390 \pm 0.032$ ps [3].

Acknowledgements

We express our gratitude to our colleagues in the CERN accelerator departments for the excellent performance of the LHC. We thank the technical and administrative staff at CERN and at the LHCb institutes, and acknowledge support from the National Agencies: CAPES, CNPq, FAPERJ and FINEP (Brazil); CERN; NSFC (China); CNRS/IN2P3 (France); BMBF, DFG, HGF and MPG (Germany); SFI (Ireland); INFN (Italy); FOM and NWO (The Netherlands); SCSR (Poland); ANCS (Romania); MinES of Russia and Rosatom (Russia); MICINN, XuntaGal and GENCAT (Spain); SNSF and SER (Switzerland); NAS Ukraine (Ukraine); STFC (United Kingdom); NSF (USA). We also acknowledge the support received from the ERC under FP7 and the Region Auvergne.

Open access

This article is published Open Access at sciencedirect.com. It is distributed under the terms of the Creative Commons Attribution License 3.0, which permits unrestricted use, distribution, and reproduction in any medium, provided the original authors and source are credited.

References

- [1] Y. Grossman, Phys. Lett. B 380 (1996) 99, arXiv:hep-ph/9603244.
- [2] A. Lenz, U. Nierste, JHEP 0706 (2007) 072, arXiv:hep-ph/0612167.
- [3] R. Fleischer, R. Kneijens, Eur. Phys. J. C 71 (2011) 1532, arXiv:hep-ph/1011.1096.
- [4] R. Fleischer, Eur. Phys. J. C 52 (2007) 267, arXiv:hep-ph/0705.1121.
- [5] A. Abulencia, et al., CDF Collaboration, Phys. Rev. Lett. 97 (2006) 211802, arXiv:hep-ex/0607021.
- [6] CDF Collaboration, Measurement of branching fractions and direct CP asymmetries of $B_{(s)}^0 \rightarrow h^+h'^-$ decays in 1 fb^{-1} , CDF public note 8579v1.
- [7] C.-C. Peng, et al., Belle Collaboration, Phys. Rev. D 82 (2010) 072007, arXiv:hep-ex/1006.5115.
- [8] K. Nakamura, et al., Particle Data Group, J. Phys. G 37 (2010) 075021.
- [9] K. Hartkorn, H.G. Moser, Eur. Phys. J. C 8 (1999) 381.
- [10] A. Lenz, U. Nierste, Numerical updates of lifetimes and mixing parameters of B mesons, in: Proceedings of the 6th International Workshop on the CKM Unitarity Triangle, 2010, in press, arXiv:hep-ph/1102.4274.
- [11] A.A. Alves Jr., et al., LHCb Collaboration, JINST 3 (2008) S08005.
- [12] R. Bailey, et al., Z. Phys. C 28 (1985) 357.
- [13] J. Rademacker, Nucl. Instrum. Meth. A 570 (2007) 525, arXiv:hep-ex/0502042.
- [14] T. Aaltonen, et al., CDF Collaboration, Phys. Rev. D 83 (2011) 032008, arXiv:hep-ex/1004.4855.
- [15] V.V. Gligorov, Measurement of the CKM angle γ and B meson lifetimes at the LHCb detector, University of Oxford, CERN-THESIS-2008-044, 2007.
- [16] M. Gersabeck, Alignment of the LHCb vertex locator and lifetime measurements of two-body hadronic final states, University of Glasgow, CERN-THESIS-2009-118, 2009.
- [17] K. Cranmer, Comput. Phys. Commun. 136 (2001) 198, arXiv:hep-ex/0011057.
- [18] LHCb Collaboration, Measurement of the CP violation parameter A_F in two-body charm decays, LHCb-CONF-2011-046, 2011.
- [19] A. Powell, PoS (ICHEP 2010) 020.
- [20] T. Skwarnicki, A study of the radiative cascade transitions between the upsilon-prime and upsilon resonances, PhD thesis, DESY F31-86-02, 1986, Appendix E.

LHCb Collaboration

R. Aaij²³, C. Abellan Beteta^{35,n}, B. Adeva³⁶, M. Adinolfi⁴², C. Adrover⁶, A. Affolder⁴⁸, Z. Ajaltouni⁵, J. Albrecht³⁷, F. Alessio³⁷, M. Alexander⁴⁷, G. Alkhazov²⁹, P. Alvarez Cartelle³⁶, A.A. Alves Jr.²², S. Amato², Y. Amhis³⁸, J. Anderson³⁹, R.B. Appleby⁵⁰, O. Aquines Gutierrez¹⁰, F. Archilli^{18,37}, L. Arrabito⁵³, A. Artamonov³⁴, M. Artuso^{52,37}, E. Aslanides⁶, G. Auriemma^{22,m}, S. Bachmann¹¹, J.J. Back⁴⁴, D.S. Bailey⁵⁰, V. Balagura^{30,37}, W. Baldini¹⁶, R.J. Barlow⁵⁰, C. Barschel³⁷, S. Barsuk⁷,

W. Barter⁴³, A. Bates⁴⁷, C. Bauer¹⁰, Th. Bauer²³, A. Bay³⁸, I. Bediaga¹, S. Belogurov³⁰, K. Belous³⁴, I. Belyaev^{30,37}, E. Ben-Haim⁸, M. Benayoun⁸, G. Bencivenni¹⁸, S. Benson⁴⁶, J. Benton⁴², R. Bernet³⁹, M.-O. Bettler¹⁷, M. van Beuzekom²³, A. Bien¹¹, S. Bifani¹², A. Bizzeti^{17,h}, P.M. Bjørnstad⁵⁰, T. Blake³⁷, F. Blanc³⁸, C. Blanks⁴⁹, J. Blouw¹¹, S. Blusk⁵², A. Bobrov³³, V. Bocci²², A. Bondar³³, N. Bondar²⁹, W. Bonivento¹⁵, S. Borghi⁴⁷, A. Borgia⁵², T.J.V. Bowcock⁴⁸, C. Bozzi¹⁶, T. Brambach⁹, J. van den Brand²⁴, J. Bressieux³⁸, D. Brett⁵⁰, S. Brisbane⁵¹, M. Britsch¹⁰, T. Britton⁵², N.H. Brook⁴², H. Brown⁴⁸, A. Büchler-Germann³⁹, I. Burducea²⁸, A. Bursche³⁹, J. Buytaert³⁷, S. Cadeddu¹⁵, J.M. Caicedo Carvajal³⁷, O. Callot⁷, M. Calvi^{20,j}, M. Calvo Gomez^{35,n}, A. Camboni³⁵, P. Campana^{18,37}, A. Carbone¹⁴, G. Carboni^{21,k}, R. Cardinale^{19,37,i}, A. Cardini¹⁵, L. Carson³⁶, K. Carvalho Akiba², G. Casse⁴⁸, M. Cattaneo³⁷, M. Charles⁵¹, Ph. Charpentier³⁷, N. Chiapolini³⁹, K. Ciba³⁷, X. Cid Vidal³⁶, G. Ciezarek⁴⁹, P.E.L. Clarke^{46,37}, M. Clemencic³⁷, H.V. Cliff⁴³, J. Closier³⁷, C. Coca²⁸, V. Coco²³, J. Cogan⁶, P. Collins³⁷, A. Comerma-Montells³⁵, F. Constantin²⁸, G. Conti³⁸, A. Contu⁵¹, A. Cook⁴², M. Coombes⁴², G. Corti³⁷, G.A. Cowan³⁸, R. Currie⁴⁶, B. D'Almagne⁷, C. D'Ambrosio³⁷, P. David⁸, I. De Bonis⁴, S. De Capua^{21,k}, M. De Cian³⁹, F. De Lorenzi¹², J.M. De Miranda¹, L. De Paula², P. De Simone¹⁸, D. Decamp⁴, M. Deckenhoff⁹, H. Degaudenzi^{38,37}, M. Deissenroth¹¹, L. Del Buono⁸, C. Deplano¹⁵, D. Derkach^{14,37}, O. Deschamps⁵, F. Dettori^{15,d}, J. Dickens⁴³, H. Dijkstra³⁷, P. Diniz Batista¹, F. Domingo Bonal^{35,n}, S. Donleavy⁴⁸, F. Dordei¹¹, A. Dosil Suárez³⁶, D. Dossett⁴⁴, A. Dovbnya⁴⁰, F. Dupertuis³⁸, R. Dzhelyadin³⁴, A. Dziurda²⁵, S. Easo⁴⁵, U. Egede⁴⁹, V. Egorychev³⁰, S. Eidelman³³, D. van Eijk²³, F. Eisele¹¹, S. Eisenhardt⁴⁶, R. Ekelhof⁹, L. Eklund^{47,*}, Ch. Elsasser³⁹, D.G. d'Enterria^{35,o}, D. Esperante Pereira³⁶, L. Estève⁴³, A. Falabella^{16,e}, E. Fanchini^{20,j}, C. Färber¹¹, G. Fardell⁴⁶, C. Farinelli²³, S. Farry¹², V. Fave³⁸, V. Fernandez Albor³⁶, M. Ferro-Luzzi³⁷, S. Filippov³², C. Fitzpatrick⁴⁶, M. Fontana¹⁰, F. Fontanelli^{19,i}, R. Forty³⁷, M. Frank³⁷, C. Frei³⁷, M. Frosini^{17,37,f}, S. Furcas²⁰, A. Gallas Torreira³⁶, D. Galli^{14,c}, M. Gandelman², P. Gandini⁵¹, Y. Gao³, J.-C. Garnier³⁷, J. Garofoli⁵², J. Garra Tico⁴³, L. Garrido³⁵, D. Gascon³⁷, C. Gaspar³⁷, N. Gauvin³⁸, M. Gersabeck³⁷, T. Gershon^{44,37}, Ph. Ghez⁴, V. Gibson⁴³, V.V. Gligorov³⁷, C. Göbel⁵⁴, D. Golubkov³⁰, A. Golutvin^{49,30,37}, A. Gomes², H. Gordon⁵¹, M. Grabalosa Gándara³⁵, R. Graciani Diaz³⁵, L.A. Granado Cardoso³⁷, E. Graugés³⁵, G. Graziani¹⁷, A. Grecu²⁸, E. Greening⁵¹, S. Gregson⁴³, B. Gui⁵², E. Gushchin³², Yu. Guz³⁴, T. Gys³⁷, G. Haefeli³⁸, C. Haen³⁷, S.C. Haines⁴³, T. Hampson⁴², S. Hansmann-Menzemer¹¹, R. Harji⁴⁹, N. Harnew⁵¹, J. Harrison⁵⁰, P.F. Harrison⁴⁴, J. He⁷, V. Heijne²³, K. Hennessy⁴⁸, P. Henrard⁵, J.A. Hernando Morata³⁶, E. van Herwijnen³⁷, E. Hicks⁴⁸, K. Holubyev¹¹, P. Hopchev⁴, W. Hulsbergen²³, P. Hunt⁵¹, T. Huse⁴⁸, R.S. Huston¹², D. Hutchcroft⁴⁸, D. Hynds⁴⁷, V. Iakovenko⁴¹, P. Ilten¹², J. Imong⁴², R. Jacobsson³⁷, A. Jaeger¹¹, M. Jahjah Hussein⁵, E. Jans²³, F. Jansen²³, P. Jaton³⁸, B. Jean-Marie⁷, F. Jing³, M. John⁵¹, D. Johnson⁵¹, C.R. Jones⁴³, B. Jost³⁷, M. Kaballo⁹, S. Kandybei⁴⁰, M. Karacson³⁷, T.M. Karbach⁹, J. Keaveney¹², U. Kerzel³⁷, T. Ketel²⁴, A. Keune³⁸, B. Khanji⁶, Y.M. Kim⁴⁶, M. Knecht³⁸, S. Koblitz³⁷, P. Koppenburg²³, A. Kozlinskiy²³, L. Kravchuk³², K. Kreplin¹¹, M. Kreps⁴⁴, G. Krocker¹¹, P. Krokovny¹¹, F. Kruse⁹, K. Kruzelecki³⁷, M. Kucharczyk^{20,25,37,j}, R. Kumar^{14,37}, T. Kvaratskheliya^{30,37}, V.N. La Thi³⁸, D. Lacarrere³⁷, G. Lafferty⁵⁰, A. Lai¹⁵, D. Lambert⁴⁶, R.W. Lambert³⁷, E. Lanciotti³⁷, G. Lanfranchi¹⁸, C. Langenbruch¹¹, T. Latham⁴⁴, R. Le Gac⁶, J. van Leerdam²³, J.-P. Lees⁴, R. Lefèvre⁵, A. Leflat^{31,37}, J. Lefrançois⁷, O. Leroy⁶, T. Lesiak²⁵, L. Li³, L. Li Gioi⁵, M. Lieng⁹, M. Liles⁴⁸, R. Lindner³⁷, C. Linn¹¹, B. Liu³, G. Liu³⁷, J.H. Lopes², E. Lopez Asamar³⁵, N. Lopez-March³⁸, J. Luisier³⁸, F. Machefert⁷, I.V. Machikhiliyan^{4,30}, F. Maciuc¹⁰, O. Maev^{29,37}, J. Magnin¹, S. Malde⁵¹, R.M.D. Mamunur³⁷, G. Manca^{15,d}, G. Mancinelli⁶, N. Mangiafave⁴³, U. Marconi¹⁴, R. Märki³⁸, J. Marks¹¹, G. Martellotti²², A. Martens⁷, L. Martin⁵¹, A. Martín Sánchez⁷, D. Martinez Santos³⁷, A. Massafferri¹, Z. Mathe¹², C. Matteuzzi²⁰, M. Matveev²⁹, E. Maurice⁶, B. Maynard⁵², A. Mazurov^{16,32,37}, G. McGregor⁵⁰, R. McNulty¹², C. Mclean¹⁴, M. Meissner¹¹, M. Merk²³, J. Merkel⁹, R. Messi^{21,k}, S. Miglioranza³⁷, D.A. Milanese^{13,37}, M.-N. Minard⁴, S. Monteil⁵, D. Moran¹², P. Morawski²⁵, R. Mountain⁵², I. Mous²³, F. Muheim⁴⁶, K. Müller³⁹, R. Muresan^{28,38}, B. Muryn²⁶, M. Musy³⁵, J. Mylroie-Smith⁴⁸, P. Naik⁴², T. Nakada³⁸, R. Nandakumar⁴⁵, J. Nardulli⁴⁵, I. Nasteva¹, M. Nedos⁹, M. Needham⁴⁶, N. Neufeld³⁷, C. Nguyen-Mau^{38,p}, M. Nicol⁷, S. Nies⁹, V. Niess⁵, N. Nikitin³¹, A. Nomerotski⁵¹, A. Novoselov³⁴, A. Oblakowska-Mucha²⁶, V. Obraztsov³⁴, S. Oggero²³, S. Ogilvy⁴⁷, O. Okhrimenko⁴¹, R. Oldeman^{15,d}, M. Orlandea²⁸, J.M. Otalora Goicochea², P. Owen⁴⁹, K. Pal⁵², J. Palacios³⁹, A. Palano^{13,b}, M. Palutan¹⁸, J. Panman³⁷, A. Papanestis⁴⁵, M. Pappagallo^{13,b},

C. Parkes^{47,37}, C.J. Parkinson⁴⁹, G. Passaleva¹⁷, G.D. Patel⁴⁸, M. Patel⁴⁹, S.K. Paterson⁴⁹, G.N. Patrick⁴⁵, C. Patrignani^{19,i}, C. Pavel-Nicorescu²⁸, A. Pazos Alvarez³⁶, A. Pellegrino²³, G. Penso^{22,l}, M. Pepe Altarelli³⁷, S. Perazzini^{14,c}, D.L. Perego^{20,j}, E. Perez Trigo³⁶, A. Pérez-Calero Yzquierdo³⁵, P. Perret⁵, M. Perrin-Terrin⁶, G. Pessina²⁰, A. Petrella^{16,37}, A. Petrolini^{19,i}, E. Picatoste Olloqui³⁵, B. Pie Valls³⁵, B. Pietrzyk⁴, T. Pilar⁴⁴, D. Pinci²², R. Plackett⁴⁷, S. Playfer⁴⁶, M. Plo Casasus³⁶, G. Polok²⁵, A. Poluektov^{44,33}, E. Polycarpo², D. Popov¹⁰, B. Popovici²⁸, C. Potterat³⁵, A. Powell⁵¹, T. du Pree²³, J. Prisciandaro³⁸, V. Pugatch⁴¹, A. Puig Navarro³⁵, W. Qian⁵², J.H. Rademacker⁴², B. Rakotomiamanana³⁸, M.S. Rangel², I. Raniuk⁴⁰, G. Raven²⁴, S. Redford⁵¹, M.M. Reid⁴⁴, A.C. dos Reis¹, S. Ricciardi⁴⁵, K. Rinnert⁴⁸, D.A. Roa Romero⁵, P. Robbe⁷, E. Rodrigues⁴⁷, F. Rodrigues², P. Rodriguez Perez³⁶, G.J. Rogers⁴³, S. Roiser³⁷, V. Romanovsky³⁴, M. Rosello^{35,n}, J. Rouvinet³⁸, T. Ruf³⁷, H. Ruiz³⁵, G. Sabatino^{21,k}, J.J. Saborido Silva³⁶, N. Sagidova²⁹, P. Sail⁴⁷, B. Saitta^{15,d}, C. Salzmann³⁹, M. Sannino^{19,i}, R. Santacesaria²², C. Santamarina Rios³⁶, R. Santinelli³⁷, E. Santovetti^{21,k}, M. Sapunov⁶, A. Sarti^{18,l}, C. Satriano^{22,m}, A. Satta²¹, M. Savrie^{16,e}, D. Savrina³⁰, P. Schaack⁴⁹, M. Schiller¹¹, S. Schleich⁹, M. Schmelling¹⁰, B. Schmidt³⁷, O. Schneider³⁸, A. Schopper³⁷, M.-H. Schune⁷, R. Schwemmer³⁷, B. Sciascia¹⁸, A. Sciubba^{18,l}, M. Seco³⁶, A. Semennikov³⁰, K. Senderowska²⁶, I. Sepp⁴⁹, N. Serra³⁹, J. Serrano⁶, P. Seyfert¹¹, B. Shao³, M. Shapkin³⁴, I. Shapoval^{40,37}, P. Shatalov³⁰, Y. Shcheglov²⁹, T. Shears⁴⁸, L. Shekhtman³³, O. Shevchenko⁴⁰, V. Shevchenko³⁰, A. Shires⁴⁹, R. Silva Coutinho⁵⁴, H.P. Skottowe⁴³, T. Skwarnicki⁵², A.C. Smith³⁷, N.A. Smith⁴⁸, E. Smith^{51,45}, K. Sobczak⁵, F.J.P. Soler⁴⁷, A. Solomin⁴², F. Soomro¹⁸, B. Souza De Paula², B. Spaan⁹, A. Sparkes⁴⁶, P. Spradlin⁴⁷, F. Stagni³⁷, S. Stahl¹¹, O. Steinkamp³⁹, S. Stoica²⁸, S. Stone^{52,37}, B. Storaci²³, M. Straticiu²⁸, U. Straumann³⁹, N. Styles⁴⁶, V.K. Subbiah³⁷, S. Swientek⁹, M. Szczekowski²⁷, P. Szczypka³⁸, T. Szumlak²⁶, S. T'Jampens⁴, E. Teodorescu²⁸, F. Teubert³⁷, C. Thomas⁵¹, E. Thomas³⁷, J. van Tilburg¹¹, V. Tisserand⁴, M. Tobin³⁹, S. Topp-Joergensen⁵¹, N. Torr⁵¹, E. Tournefier^{4,49}, M.T. Tran³⁸, A. Tsaregorodtsev⁶, N. Tuning²³, M. Ubeda Garcia³⁷, A. Ukleja²⁷, P. Urquijo⁵², U. Uwer¹¹, V. Vagnoni¹⁴, G. Valenti¹⁴, R. Vazquez Gomez³⁵, P. Vazquez Regueiro³⁶, S. Vecchi¹⁶, J.J. Velthuis⁴², M. Veltri^{17,g}, K. Vervink³⁷, B. Viaud⁷, I. Videau⁷, X. Vilasis-Cardona^{35,n}, J. Visniakov³⁶, A. Vollhardt³⁹, D. Voong⁴², A. Vorobyev²⁹, H. Voss¹⁰, K. Wacker⁹, S. Wandernoth¹¹, J. Wang⁵², D.R. Ward⁴³, A.D. Webber⁵⁰, D. Websdale⁴⁹, M. Whitehead⁴⁴, D. Wiedner¹¹, L. Wiggers²³, G. Wilkinson⁵¹, M.P. Williams^{44,45}, M. Williams⁴⁹, F.F. Wilson⁴⁵, J. Wishahi⁹, M. Witek²⁵, W. Witzeling³⁷, S.A. Wotton⁴³, K. Wyllie³⁷, Y. Xie⁴⁶, F. Xing⁵¹, Z. Xing⁵², Z. Yang³, R. Young⁴⁶, O. Yushchenko³⁴, M. Zavertyaev^{10,a}, F. Zhang³, L. Zhang⁵², W.C. Zhang¹², Y. Zhang³, A. Zhelezov¹¹, L. Zhong³, E. Zverev³¹, A. Zvyagin³⁷

¹ Centro Brasileiro de Pesquisas Físicas (CBPF), Rio de Janeiro, Brazil

² Universidade Federal do Rio de Janeiro (UFRJ), Rio de Janeiro, Brazil

³ Center for High Energy Physics, Tsinghua University, Beijing, China

⁴ LAPP, Université de Savoie, CNRS/IN2P3, Annecy-Le-Vieux, France

⁵ Clermont Université, Université Blaise Pascal, CNRS/IN2P3, LPC, Clermont-Ferrand, France

⁶ CPPM, Aix-Marseille Université, CNRS/IN2P3, Marseille, France

⁷ LAL, Université Paris-Sud, CNRS/IN2P3, Orsay, France

⁸ LPNHE, Université Pierre et Marie Curie, Université Paris Diderot, CNRS/IN2P3, Paris, France

⁹ Fakultät Physik, Technische Universität Dortmund, Dortmund, Germany

¹⁰ Max-Planck-Institut für Kernphysik (MPIK), Heidelberg, Germany

¹¹ Physikalisches Institut, Ruprecht-Karls-Universität Heidelberg, Heidelberg, Germany

¹² School of Physics, University College Dublin, Dublin, Ireland

¹³ Sezione INFN di Bari, Bari, Italy

¹⁴ Sezione INFN di Bologna, Bologna, Italy

¹⁵ Sezione INFN di Cagliari, Cagliari, Italy

¹⁶ Sezione INFN di Ferrara, Ferrara, Italy

¹⁷ Sezione INFN di Firenze, Firenze, Italy

¹⁸ Laboratori Nazionali dell'INFN di Frascati, Frascati, Italy

¹⁹ Sezione INFN di Genova, Genova, Italy

²⁰ Sezione INFN di Milano Bicocca, Milano, Italy

²¹ Sezione INFN di Roma Tor Vergata, Roma, Italy

²² Sezione INFN di Roma La Sapienza, Roma, Italy

²³ Nikhef National Institute for Subatomic Physics, Amsterdam, Netherlands

²⁴ Nikhef National Institute for Subatomic Physics and Vrije Universiteit, Amsterdam, Netherlands

²⁵ Henryk Niewodniczanski Institute of Nuclear Physics Polish Academy of Sciences, Cracow, Poland

²⁶ Faculty of Physics & Applied Computer Science, Cracow, Poland

²⁷ Soltan Institute for Nuclear Studies, Warsaw, Poland

²⁸ Horia Hulubei National Institute of Physics and Nuclear Engineering, Bucharest-Magurele, Romania

²⁹ Petersburg Nuclear Physics Institute (PNPI), Gatchina, Russia

³⁰ Institute of Theoretical and Experimental Physics (ITEP), Moscow, Russia

- ³¹ Institute of Nuclear Physics, Moscow State University (SINP MSU), Moscow, Russia
³² Institute for Nuclear Research of the Russian Academy of Sciences (INR RAN), Moscow, Russia
³³ Budker Institute of Nuclear Physics (SB RAS) and Novosibirsk State University, Novosibirsk, Russia
³⁴ Institute for High Energy Physics (IHEP), Protvino, Russia
³⁵ Universitat de Barcelona, Barcelona, Spain
³⁶ Universidad de Santiago de Compostela, Santiago de Compostela, Spain
³⁷ European Organization for Nuclear Research (CERN), Geneva, Switzerland
³⁸ Ecole Polytechnique Fédérale de Lausanne (EPFL), Lausanne, Switzerland
³⁹ Physik-Institut, Universität Zürich, Zürich, Switzerland
⁴⁰ NSC Kharkiv Institute of Physics and Technology (NSC KIPT), Kharkiv, Ukraine
⁴¹ Institute for Nuclear Research of the National Academy of Sciences (KINR), Kyiv, Ukraine
⁴² H.H. Wills Physics Laboratory, University of Bristol, Bristol, United Kingdom
⁴³ Cavendish Laboratory, University of Cambridge, Cambridge, United Kingdom
⁴⁴ Department of Physics, University of Warwick, Coventry, United Kingdom
⁴⁵ STFC Rutherford Appleton Laboratory, Didcot, United Kingdom
⁴⁶ School of Physics and Astronomy, University of Edinburgh, Edinburgh, United Kingdom
⁴⁷ School of Physics and Astronomy, University of Glasgow, Glasgow, United Kingdom
⁴⁸ Oliver Lodge Laboratory, University of Liverpool, Liverpool, United Kingdom
⁴⁹ Imperial College London, London, United Kingdom
⁵⁰ School of Physics and Astronomy, University of Manchester, Manchester, United Kingdom
⁵¹ Department of Physics, University of Oxford, Oxford, United Kingdom
⁵² Syracuse University, Syracuse, NY, United States
⁵³ CC-IN2P3, CNRS/IN2P3, Lyon-Villeurbanne, France ^q
⁵⁴ Pontifícia Universidade Católica do Rio de Janeiro (PUC-Rio), Rio de Janeiro, Brazil ^r

* Corresponding author.

E-mail address: Lars.Eklund@cern.ch (L. Eklund).

^a P.N. Lebedev Physical Institute, Russian Academy of Science (LPI RAS), Moscow, Russia.

^b Università di Bari, Bari, Italy.

^c Università di Bologna, Bologna, Italy.

^d Università di Cagliari, Cagliari, Italy.

^e Università di Ferrara, Ferrara, Italy.

^f Università di Firenze, Firenze, Italy.

^g Università di Urbino, Urbino, Italy.

^h Università di Modena e Reggio Emilia, Modena, Italy.

ⁱ Università di Genova, Genova, Italy.

^j Università di Milano Bicocca, Milano, Italy.

^k Università di Roma Tor Vergata, Roma, Italy.

^l Università di Roma La Sapienza, Roma, Italy.

^m Università della Basilicata, Potenza, Italy.

ⁿ LIFAELS, La Salle, Universitat Ramon Llull, Barcelona, Spain.

^o Institució Catalana de Recerca i Estudis Avançats (ICREA), Barcelona, Spain.

^p Hanoi University of Science, Hanoi, Viet Nam.

^q Associated member.

^r Associated to Universidade Federal do Rio de Janeiro (UFRJ), Rio de Janeiro, Brazil.